ENDOR and ESEEM Investigation of $Ag^{I}_2Cu^{II}_2$ Bovine Superoxide Dismutase

Ryszard J. Gurbiel,[†,§] Risa Peoples,[‡] Peter E. Doan,[†] John F. Cline,[†] John McCracken,[∥] Jack Peisach,[⊥] Brian M. Hoffman,[†] and Joan Selverstone Valentine*[,‡]

Department of Chemistry, Northwestern University, Evanston, Illinois 60208, Department of Chemistry and Biochemistry, University of California, Los Angeles, California 90024, Department of Molecular Pharmacology, Albert Einstein College of Medicine, Bronx, New York 10461, Department of Chemistry, Michigan State University, East Lansing, Michigan 48824, and Department of Molecular Biology, Jagiellonian University, 31-120 Kraków, Poland

Received July 17, 1992

$Ag^{I}_2Cu^{II}_2$SOD, a derivative of bovine superoxide dismutase containing Ag and Cu rather than Cu and Zn, has been studied by a wide range of paramagnetic resonance techniques. Evidence based on the linear electric field effect (LEFE) in pulsed EPR supports the original conclusion that Cu(II) occupies the Zn(II) site of the native protein, substantially retaining the pseudo-tetrahedral coordination geometry. Cw ENDOR investigation at X (9 GHz) and Q (35 GHz) bands and pulsed ENDOR at X band demonstrate at least two populations of imidazole-^{14}N directly coordinated to Cu(II) in the Zn(II) site, one with an isotropic hyperfine coupling of about 42 MHz, normal for Cu imidazole complexes, and the other, which is inferred to have two members, with a coupling of about 28 MHz. Electron spin echo envelope modulation (ESEEM) investigation also detects two populations of remote ^{14}N of imidazole coupled to Cu(II). One population consists of a single ^{14}N with an isotropic hyperfine coupling constant of about 2.0 MHz and is assigned to the imidazole with the 42-MHz coupling. The second population has a coupling of about 1 MHz and is assigned to imidazole with the 28-MHz coupling. This investigation demonstrates that Cu(II) forms inequivalent bonds to the three imidazoles in the distorted tetrahedral environment of the Zn(II) site and is consistent with the view that a bimetallic imidazolate bridge found in the native Cu_2Zn_2 protein is broken in $Ag^{I}_2Cu^{II}_2$SOD.

Bovine copper–zinc superoxide dismutase ($Cu^{II}_2Zn^{II}_2$SOD)[1] contains two identical polypeptide subunits, each of which contains one copper and one zinc atom.[2,3] X-ray crystallographic analysis[4–6] shows that the Zn(II) is bound to the imidazole side chains of His 69 and 78, to a carbonyl side chain of Asp 81, and to the imidazole side chain of His 61, the last of which is deprotonated and forms a bridge between Cu(II) and Zn(II). The Cu(II) is coordinated to the bridge and to three other histidyl residues (His 44, 46, and 118) (Figure 1). Under appropriate conditions, the native metal ions can be reversibly removed from the protein, and a number of protocols have been developed whereby various other metal ions can be individually bound at the native copper and zinc binding sites originating in the holo protein.[3]

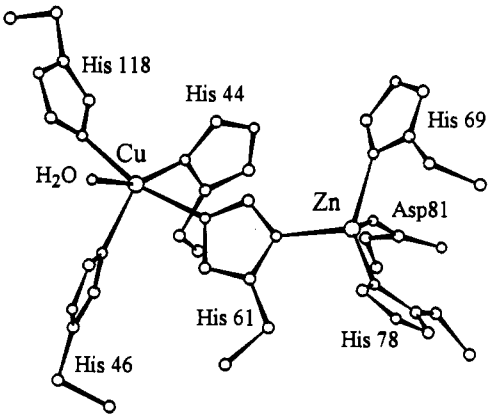

Figure 1. Schematic representation of the active site of bound $Cu^{II}_2Zn^{II}_2$SOD.[4–6] The derivative that is the subject of this paper has Cu(II) substituted for Zn(II) and Ag(I) substituted for Cu(II).

EPR spectroscopy has been used to study the properties of the copper-binding sites in $Cu^{II}_2Zn^{II}_2$SOD[7,8] as well as in the $Ag(I)_2$-Cu^{II}_2 derivative,[9] which contains diamagnetic Ag(I) at the copper site and Cu^{II} at the zinc site of the native protein.[10] The EPR spectra and corresponding spin Hamiltonian parameters of Cu(II) in $Ag^{I}_2Cu^{II}_2$SOD are unusual compared to most non-blue copper-containing proteins, as are those of one of the type 3 coppers in tree laccase.[12] This can be recognized from their positions on

[†] Northwestern University.
[§] Jagiellonian University.
[‡] University of California.
[∥] Michigan State University.
[⊥] Albert Einstein College of Medicine.

(1) Abbreviations: SOD, the native form of cuprozinc superoxide dismutase as isolated from bovine liver. X_2Y_2SOD signifies those derivatives of the native protein in which the metal ions X and Y have been substituted for the native Cu^{2+} and Zn^{2+}, respectively (X and Y may be the same: E = empty). All metal ions are assumed to be 2+ unless noted otherwise, except for silver which has an oxidation state of 1+. ESEEM, electron spin echo envelope modulation; cw, continuous wave; NQR, nuclear quadrupole resonance; imid, imidazole; ENDOR, electron nuclear double resonance.

(2) (a) Fridovich, I. *Adv. Enzymol. Relat. Areas Mol. Biol.* **1987**, *58*, 61–97. (b) Banci, L.; Bertini, I.; Luchinat, C.; Piccioli, M. *Coord. Chem. Rev.* **1990**, *100*, 67–103.
(3) Valentine, J. S.; Pantoliano, M. W. *Copper Proteins*; Spiro, T. G., Ed.; Wiley: New York, 1981; Chapter 8, pp 291–358.
(4) Tainer, J. A.; Getzoff, E. D.; Beem, K. M.; Richardson, J. S.; Richardson, D. C. *J. Mol. Biol.* **1982**, *160*, 181–217.
(5) Tainer, J. A.; Getzoff, E. D.; Richardson, J. S.; Richardson, D. C. *Nature* **1983**, *306*, 284–287.
(6) Getzoff, E. D.; Tainer, J. A.; Weiner, P. K.; Kollman, P. A.; Richardson, J. S.; Richardson, D. C. *Nature* **1983**, *306*, 287–290.
(7) Pantoliano, M. W.; Valentine, J. S.; Nafie, L. A. *J. Am. Chem. Soc.* **1982**, *104*, 6310–6317.
(8) Liberman, R. A.; Sands, R. H.; Fee, J. A. *J. Biol. Chem.* **1982**, *257*, 336–344.
(9) Beem, K. M.; Richardson, D. C.; Rajagopalan, K. U. *Biochemistry* **1977**, *16*, 1930–1936.
(10) Roe, J. A.; Peoples, R.; Scholler, D. M.; Valentine, J. S. *J. Am. Chem. Soc.* **1990**, *112*, 1538–1545.

0020-1669/93/1332-1813$04.00/0 © 1993 American Chemical Society

a plot of $g_{\|}$ versus $A_{\|}$.[7,11] These Cu(II) sites, along with Cu_B of cytochrome *c* oxidase,[12] fall in a class intermediate between the "typical" near-tetragonally coordinated type 2 and the type 1 blue copper proteins. The similarity in their EPR parameters may have a chemical basis, because ^{14}N ENDOR studies showed three different nitrogen couplings for one of the copper atoms constituting the type 3 site in tree laccase,[13] whereas the Zn binding site in SOD contains three imidazoles.[4-6]

We have collected cw and pulsed ENDOR and ESEEM spectra of Ag_2Cu_2SOD in order to compare imidazole binding to copper coordinated in the structurally-defined zinc site of this protein with that of the previously studied type 3 copper in tree laccase, as well as with Cu_B in cytochrome *c* oxidase, copper in native $Cu^{II}_2Zn^{II}_2SOD$, and copper in blue copper proteins. The ENDOR spectra presented here for Ag_2Cu_2SOD arise from two distinct populations of directly coordinated ^{14}N of imidazoles, one having a hyperfine coupling typical of Cu(II)–imid models and a number of Cu proteins,[15,16] the other likely comprised of two members, having an appreciably smaller coupling. ESEEM spectroscopic examination of the remote ^{14}N of coordinated imidazole also demonstrates two populations of imidazoles. One of these consists of a single imidazole whose remote ^{14}N has a magnetic coupling resembling that in the Cu(II)–imid models and in a number of copper proteins,[17-21] and that clearly is associated with the more strongly coupled coordinated ^{14}N seen in ENDOR. The data thus indicate that the Cu(II) at the zinc binding site of SOD binds three imidazoles, but with two weak Cu–N bonds, rather than three equivalent bonds.

Materials and Methods

The Ag(I)–Cu(II) derivative of bovine erythrocuprin SOD was prepared by modification of the procedure of Beem et al.[9] The sample contained a small amount ($\lesssim$10%) of the native $Cu^{II}_2Zn^{II}_2SOD$, which did not give detectable contributions to the ENDOR or ESEEM.

The cw and pulsed ENDOR spectra were obtained at 2 K at Northwestern University on locally constructed spectrometers that are described elsewhere.[22-24] The cw ENDOR signals were observed as a decrease in the 100-kHz modulated, dispersion mode EPR signal. All cw ENDOR patterns were observed with both increasing and decreasing frequency sweeps; parameters reported are the average of these measurements. Pulsed ENDOR spectra were obtained using a Davies sequence.[25] In that method a microwave π pulse (t_p) first inverts polarization of an electron spin transition. A radio frequency (rf) π pulse is then applied to the appropriate nuclear transition to induce sub-level polarization transfer. The final electron spin polarization is detected as the spin echo intensity generated in a subsequent two-pulse detection sequence. It was shown[24,26] that the ENDOR response for nucleus J with the coupling A^J varies with the selectivity parameter (η_J) through the relationship shown in eq 1.

$$I(\eta_J) = \frac{1.4 I_0{}^J \eta_J}{(0.7)^2 + \eta_J{}^2} \tag{1a}$$

$$\eta_J = A^J t_p \tag{1b}$$

Consider a system where a proton, H, and heteronucleus, N (e.g., ^{14}N) have overlapping ENDOR signals but the hyperfine couplings obey the relation $\alpha \equiv A^N/A^H \gg 1$. The relative intensity of those signals can be chosen through proper selection of the duration of the first pulse (t_p). In the limiting case of $\eta_N = A^N t_p{}^N \to 0$ the relative intensities of those two signals approach the value $\alpha I_0{}^N/I_0{}^H \sim \alpha^2$. In practice, by applying a very short inverting pulse t_p it is possible to reduce the intensity of the proton signal below the level of detectability while optimizing signals from, e.g., a strongly coupled ^{14}N. This approach has been denoted the PrOton Suppression, Heteronuclear Enhancement (POSHE) technique,[26] but can be applied to any case where one wishes to distinguish overlapping spectral contributions of strongly and weakly coupled nuclei.

The first-order ^{14}N ENDOR spectrum for a single orientation of a paramagnetic center consists, in principle, of four transitions at frequencies given by eq 2,[27,28] where A and P are the angle-dependent hyperfine and

$$\nu_{\pm,m}(^{14}N) = |A(^{14}N)/2 \pm \nu(^{14}N) + 3P(^{14}N)/(2m-1)| \tag{2}$$

quadrupole coupling constants, respectively, $m = 1, 0$, and $\nu(^{14}N)$ is the nuclear Larmor frequency, $h\nu(^{14}N) = g(^{14}N)\beta_n H_0$.[22] When, as found here, $A(^{14}N)/2 > \nu(^{14}N)$, $P(^{14}N)$, eq 2 in principle describes a four-line pattern centered at $A(^{14}N)/2$, consisting of a Larmor-split doublet further split by the quadrupolar term. The quadrupole coupling of an imidazole ^{14}N directly bound to Cu(II) typically is not resolved,[13-16] although there is one such report.[46] Thus, only a single Larmor-split doublet centered at a frequency $A(^{14}N)/2$ is expected.

The nitrogen ENDOR patterns are usually centered at frequency determined by the hyperfine coupling constant, a molecular parameter, whereas a set of magnetically equivalent protons gives a pair of ENDOR transitions ($\nu_\pm$) centered about the free-proton Larmor frequency,

$$\nu_\pm = |\nu(H) + A(H)/2| \tag{3}$$

$\nu_H = (g_H\beta_n/\beta_e)(\nu(M)/g_{obs})$, which varies with the EPR spectrometer frequency. For a fixed g_{obs} the center of the proton resonance pattern shifts in proportion to the microwave frequency $\nu(M)$. An increase of $\nu(M)$ from 9 GHz (X-band) to 35 GHz (Q-band) increases ν_H (at $g \sim 2$) from $\sim$14 MHz to $\sim$53 MHz, which eliminates spectral overlap of proton signals with those of ^{14}N (or other nuclei).

The samples employed in this study are frozen solutions and thus contain a random distribution of all protein orientations. However, an ENDOR spectrum or an ESEEM spectrum taken with the magnetic field set at any field within the EPR envelope represents a well-defined subset of molecular orientations and we have shown how to use a set of such ENDOR spectra to determine the principal values of a hyperfine tensor and its orientation relative to the **g** tensor axis frame.[29]

The pulsed EPR spectrometer used to perform LEFE and ESEEM measurements at the Albert Einstein Medical College has been described elsewhere.[30] LEFE measurements were carried out according to the method of Mims.[31] Protein samples were pipetted into the two wells on either side of a brass, LEFE cavity which was then cooled in liquid N_2. Excess sample that protruded above the dipole resonator in the cavity was scraped off with a metal blade, leaving two prisms of frozen protein

(11) Peisach, J.; Blumberg, W. E. *Arch. Biochem. Biophys.* **1974**, *165*, 691–708.
(12) Reinhammer, B.; Malkin, R.; Karlsson, B.; Andresson, L. E.; Aasa, R.; Vanngard, T.; Malmstrom, B. G. *J. Biol. Chem.* **1980**, *255*, 5000–5003.
(13) Cline, J.; Reinhammar, B.; Jensen, P.; Venters, R.; Hoffman, B. M. *J. Biol. Chem.* **1983**, *258*, 5124–5128.
(14) Werst, M. M.; Davoust, C. E.; Hoffman, B. M. *J. Am. Chem. Soc.* **1991**, *113*, 1533–1538.
(15) Van Camp, H. L.; Sands, R. H.; Fee, J. A. *J. Chem. Phys.* **1981**, *75*, 2098–2107.
(16) Roberts, J. E.; Cline, J. F.; Lum, V.; Freeman, H.; Gray, H. B.; Peisach, J.; Reinhammar, B.; Hoffman, B. M. *J. Am. Chem. Soc.* **1984**, *106*, 5324–5330.
(17) Mims, W. B.; Peisach, J. *J. Chem. Phys.* **1978**, *69*, 4921–4930.
(18) Mims, W. B.; Peisach, J. *J. Biol. Chem.* **1979**, *254*, 4321–4323.
(19) Fee, J. A.; Peisach, J.; Mims, W. B. *J. Biol. Chem.* **1981**, *256*, 1910–1914.
(20) Avigliano, L.; Davis, J. L.; Graziani, M. T.; Marchesini, A.; Mims, W. B.; Mondovi, B.; Peisach, J. *FEBS Lett.* **1981**, *156*, 80–84.
(21) McCracken, J.; Pember, S. O.; Benkovic, S. J.; Villafranca, J. J.; Miller, R. J.; Peisach, J. *J. Am. Chem. Soc.* **1987**, *110*, 1069–1074.
(22) Venters, R. A.; Nelson, M. J.; McLean, P.; True, A. E.; Levy, M. A.; Hoffman, B. M.; Orme-Johnson, W. H. *J. Am. Chem. Soc.* **1986**, *108*, 3487–3498.
(23) True, A. E.; Nelson, M. J.; Venters, R. A.; Orme-Johnson, W. A.; Hoffman, B. M. *J. Am. Chem. Soc.* **1988**, *110*, 1935–1943.
(24) Fan, C.; Doan, P. E.; Davoust, C. E.; Hoffman, B. M. *J. Magn. Reson.* **1992**, *98*, 62–72.
(25) Davies, E. R. *Phys. Lett.* **1974**, *47A*, 1–2.
(26) Doan, P. E.; Fan, Ch.; Davoust, C. E.; Hoffman, B. M. *J. Magn. Reson.* **1991**, *95*, 196–200.
(27) Abragam, A.; Bleaney, B. *Electron Paramagnetic Resonance of Transition Ions*; Clarendon Press: Oxford, U.K., 1970.
(28) Atherton, N. M. *Electron Spin Resonance*; John Wiley: New York, 1973.
(29) Hoffman, B. M.; Gurbiel, R. J.; Werst, M. M.; Sivaraja, M. *Advanced EPR. Applications in Biology and Biochemistry*; Hoff, A. J., Ed.; Elsevier: Amsterdam, 1989; pp 541–591.
(30) McCracken, J.; Peisach, J.; Dooley, D. M. *J. Am. Chem. Soc.* **1987**, *109*, 4064–4072.
(31) Mims, W. B. *Rev. Sci. Instrum.* **1974**, *45*, 1583–1591.
(32) Mims, W. B.; Peisach, J. *Biochemistry* **1976**, *15*, 3863–3869.

sample, each approximately 5 × 5 × 2 mm between the dipole resonator-electrode and the cavity walls.

The LEFE shift parameter σ is defined by the formula

$$\sigma = d[6f(\tau V)_{1/2}]^{-1} \quad (4)$$

where d is the thickness of the sample, f the microwave frequency and $(\tau V)_{1/2}$ the product of applied voltage and two-pulse microwave pulse spacing required to reduce the spin echo signal intensity by half.[33] The shift parameter σ corresponds to the mean fractional shift in g per unit of applied electric field, E. Data were collected at increments of magnetic field H_0 across the cw EPR absorption envelope with the electric field aligned parallel to ($E_{\parallel}H_0$) or perpendicular to ($E_{\perp}H$) the magnetic field.

A reflection cavity where a folded half-wave resonator serves as the resonant element was used for ESEEM studies.[34] ESEEM data were collected using a stimulated echo sequence (90°–τ–90°–T–90°) where the τ value was chosen to suppress modulation arising from weakly coupled protons in the sample.[35] Data were collected using the following spectrometer conditions: microwave frequency, 8.71 GHz; magnetic field strength, 3300 G; microwave pulse power, 50 W; microwave pulse width, 20 ns (full-width-half maximum); sample temperature, 4.2 K. ESEEM spectra were obtained by Fourier transformation of the echo decay envelopes using a modified version of the dead time reconstruction method of Mims.[36]

Simulations of cw-EPR spectra were carried out using the QPOWA program as obtained from Professor R. L. Belford at the Illinois EPR Resource Center. ESEEM spectral simulations used the density matrix formalism by Mims,[37] with the approximation of g-tensor isotropy removed, together with the orientation averaging scheme described earlier.[38,39] Orientations were selected for the ESEEM calculations using a parabolic search routine where both Cu(II) g-tensor anisotropy and Cu(II) hyperfine interactions were considered.[40] The spin Hamiltonian used to describe ^{14}N superhyperfine coupling consisted of terms for nuclear Zeeman, electron–nuclear hyperfine, and nuclear quadrupole interactions. The Cu(II)–^{14}N nuclear hyperfine coupling in ESEEM was constrained to be axial and cast in the form of the point dipole–dipole formalism where the coupling tensor is described by an isotropic term, A_{iso}, an effective dipole–dipole distance, r_{eff}, and two angles θ_n and ϕ_n that describe the orientation of the axial tensor with respect to the g-tensor.[40] The ^{14}N nuclear quadrupole interaction was described by five parameters: e^2qQ, the quadrupole coupling constant; η, the asymmetry parameter; and three Euler angles that relate the orientation of the quadrupole coupling tensor to the g-tensor. All computer simulations were performed on a Microvax II (Digital Equipment) computer.

Results

EPR and LEFE. The EPR spectrum of Cu(II) in $Ag^{I}_2Cu^{II}_2$-SOD[7] resembles that for partially reduced type 3 copper from tree laccase.[12] The reported spin Hamiltonian parameters are as follows:[7] g_1, 2.316; g_2, 2.118; g_3, ~2.01; A_1, 348 MHz; simulations further indicate $A_2 \approx A_3$, ~50 MHz. Because Cu(II) hyperfine splittings are only resolved for g_1, the values for A_2 and A_3 are approximate.

The EPR parameters are characteristic of Cu(II) in a non-tetragonal site. As the EPR spectrum is so different from that of Cu(II) in $Cu^{II}_2Zn^{II}_2$SOD or even Cu(II) in the protein depleted of Zn(II), this suggests that Cu(II) in $Ag^{I}_2Cu^{II}_2$SOD is bound to the site originally occupied by Zn(II). Further evidence for this surmise is based on a comparison of the optical difference spectrum of $Cu^{II}_2Zn^{II}_2$SOD with that of $Cu^{II}_2Cu^{II}_2$SOD. The resultant spectrum presumably is that of Cu(II) at the Zn(II) site. A nearly identical spectrum is seen for $Ag^{I}_2Cu^{II}_2$SOD.[7]

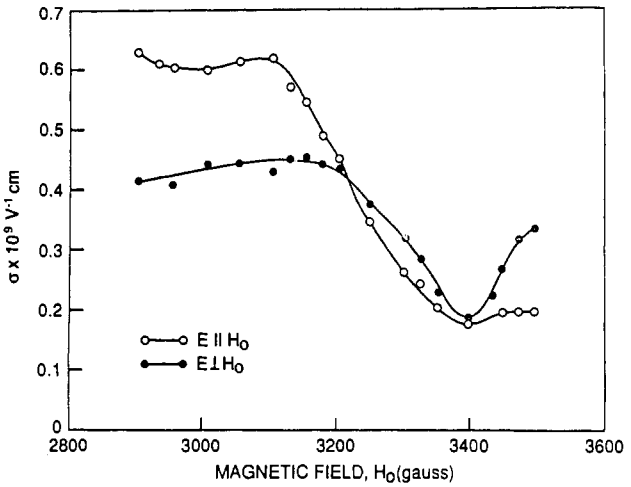

Figure 2. Linear electric field effect of $Ag^{I}_2Cu^{II}_2$SOD. Shift parameters were measured at a series of magnetic field settings with the electric field E either parallel ($E \parallel H_0$) or perpendicular ($E \perp H_0$) to the magnetic field H_0. Pulsed EPR spectrometer frequency, 9.62 GHz.

The symmetry of the Zn(II) site now occupied by Cu(II) in $Ag^{I}_2Cu^{II}_2$SOD can be further characterized by LEFE. The LEFE curves (Figure 2) bear resemblance both in shape and magnitude to those seen for near-tetrahedral Cu(II) complexes, in particular for Cu(II) *o*-phenanthroline dichloride.[33] Tetrahedrality for any tetracoordinate copper complex, as defined by Rosenberg et al.[41] can be characterized from the angle subtended by two planes, each encompassing the copper and two adjacent ligands. For strictly square planar complexes with D_{4h} symmetry the tetrahedrality is 0°. For tetrahedral complexes with D_{2d} symmetry, the tetrahedrality equals 90°. From a single crystal study of Cu(II) *o*-phenanthroline dichloride, this angle is 79°.

In a previous investigation,[33] it was suggested that the magnitude of LEFE for Cu(II) complexes could be related to the following: (1) deviation from D_{4h} symmetry toward tetrahedral; (2) irregularities in the local environment of the complex that might give rise to odd crystal field components, including orientational differences of polar molecules occupying axial coordination positions, small differences in distance to axial ligands or randomness in the glassy matrix surrounding the complex; (3) an odd ligand to copper with markedly different binding properties than the others, such as the cysteinyl sulfur ligand in azurin. As the primary structure provides no nearby cysteine and there is no indication of a S–Cu ligand-to-metal charge transfer from the optical spectrum of Ag_2Cu_2SOD,[7] one may rule out this possibility.

The magnitude of shift observed for usual square planar complexes of Cu(II) is smaller by about two-thirds[33] than seen for Ag_2Cu_2SOD or for Cu(II) *o*-phenanthroline Cl_2. We conclude, then, that the LEFE obtained for the protein is due to the distortion of the metal binding site away from that seen for simple, near-square-planar Cu(II) complexes toward that observed for near-tetrahedral complexes. From an examination of the X-ray crystal structure of Cu_2Zn_2SOD,[5] one would predict that Cu(II) replacement into the Zn binding site, with no structural rearrangement would yield a site symmetry of close to tetrahedral. Based on the criteria of Rosenberg et al.,[41] the tetrahedrality would be close to 84°.

X-Band CW ENDOR. Figure 3 presents broad-band, X-band (9.5 and 8.7 GHz) ENDOR spectra of $Ag^{I}_2Cu^{II}_2$SOD taken with the magnetic field set to g_2 of the EPR spectrum. Figure 3a, taken at a spectrometer microwave frequency of 9.5 GHz, contains an ENDOR pattern centered at the proton Larmor frequency,

(33) Peisach, J.; Mims, W. B. *Eur. J. Biochem.* **1978**, *84*, 207–214.
(34) Lin, C. P.; Bowman, M. K.; Norris, J. R. *J. Magn. Reson.* **1985**, *65*, 369–374.
(35) Mims, W. B.; Peisach, J. *Biological Magnetic Resonance*; Berliner, L. J., Reuben, J., Eds.; Plenum Press: New York, 1981; Vol. 3, pp 213–264.
(36) Mims, W. B. *J. Magn. Reson.* **1984**, *59*, 291–306.
(37) Mims, W. B. *Phys. Rev.* **1972**, *85*, 2409–2419.
(38) Hoffman, B. M.; Martinsen, J.; Venters, R. A. *J. Magn. Reson.* **1984**, *59*, 110–123.
(39) Hurst, G. C.; Henderson, T. A.; Kreilick, R. W. *J. Am. Chem. Soc.* **1985**, *107*, 7294–7299.
(40) Cornelius, J. B.; McCracken, J.; Belford, R. L.; Clarkson, R. B.; Peisach, J. *J. Phys. Chem.* **1990**, *94*, 6977–6982.
(41) Rosenberg, R. C.; Root, C. A.; Bernstein, P. K.; Gray, H. B. *J. Am. Chem. Soc.* **1975**, *97*, 2092–2096.

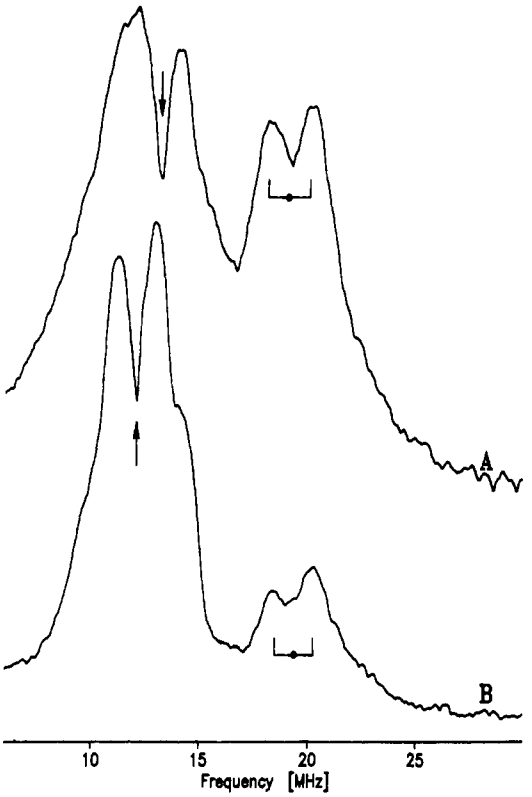

Figure 3. X-band ENDOR spectra of $Ag^{I}_2Cu^{II}_2$SOD at two microwave frequencies, with H_0 set to $\sim g_2$. Proton resonances shift with frequency, whereas the ^{14}N resonances do not. The position of the ^{14}N resonance is indicated by $A^N/2$ (·) and $2\nu_N$ (|—|). Conditions are as follows. A: microwave frequency, 9.525 GHz; H = 0.31 T; T = 2 K; microwave power, 2 μW; 100-kHz field modulation, 5 G; RF power, 20 W; RF scan rate, 5 MHz/s. B: microwave frequency, 8.7 GHz; H_0 = 0.283 T; other conditions as in (A).

ν_H. Under different conditions it is possible to resolve numerous individual proton lines characterized by hyperfine coupling constant $A^H \leq 8$ MHz. In addition there is a pair of higher frequency features that are separated by 2 MHz, which corresponds to $2\nu_N$ (eq 1), and that lack the low-frequency partners expected were they proton resonances. In Figure 3b, taken with microwave frequency at 8.7 GHz, the proton pattern has shifted appropriately to lower frequency (eq 2) and shows a change in line shape. The higher frequency features remain essentially invariant with spectrometer frequency, supporting their assignment as a Larmor-split ^{14}N doublet without resolved quadrupole splitting. Given the width of the feature, the absence of resolved quadrupole splitting in the ^{14}N resonance is consistent with previous ENDOR studies of biological copper centers having histidine imidazole nitrogen ligands.[15,16,42,43] We denote this doublet as arising from site(s) N1. As the external field is varied across the EPR spectrum the N1 resonance shifts slightly ($A \approx$ 39 MHz at g_{max} and $\approx$ 45 MHz at g_{min}), indicating that this ^{14}N coupling is primarily isotropic, but with $\sim$15% anisotropy. The average hyperfine coupling, A_{iso} = 42 MHz, is similar to that observed for Cu(II)–imid complexes[15] (Table I).

Hyperfine Selective Pulsed ENDOR. CW X-band ENDOR signals from an additional class of ^{14}N with hyperfine coupling ranging from 8 to 16 MHz would be masked by resonances from weakly coupled protons that are centered at $\nu_H \approx$ 12–14 MHz. The POSHE ENDOR technique can distinguish between such ^{14}N and ^{1}H nuclei. For example in a Davies pulsed ENDOR sequence with t_p = 32 ns the selectivity parameters are, $0 \leq \eta^H \leq 0.1$, but $0.5 \leq \eta^N \leq 1$ (eq 3). Thus, the ^{1}H signals will be strongly suppressed, to near the detectability level[24,26] compared to the ^{14}N signals, which will be near their maximum intensity.

The X-band Davies pulsed ENDOR spectrum taken with t_p = 16 ns at the low-field (g_3) edge of the EPR envelope (Figure 4a) shows a well-resolved doublet that is centered at approximately 19 MHz and arises from N1 as assigned from the cw spectra (A_3(N1) $\sim$ 38 MHz). Despite the fact that ^{1}H signals are suppressed there remains an intense but poorly resolved feature that is centered at 12.5 MHz, but which extends from $\sim$10 to $\sim$15 MHz. We assign this to nitrogen(s) N2 with the coupling(s) of $22 < A_3(N2) < 28$ MHz. As the magnetic field is increased (g-factor decreases) the N1 pair moves toward higher frequencies, as a consequence of the anisotropy of the A(N1) tensor; nitrogen(s) N2 show no detectable anisotropy (Figure 4b).

The relative intensities of pulsed ENDOR signals from two different populations of ^{14}N nuclei will reflect the relative numbers of nuclei in each class, and any experimental artifact will act to lower the intensity of the signal from the class with the smaller hyperfine coupling. Thus the higher relative intensity of the N2 signal as compared to that of N1 suggests that there are more members of the N2 class. Considering that there are three

Table I. Hyperfine Coupling Constants (MHz) of Imidazole-^{14}N Coordinated to Cu(II) Sites

$Ag^{I}_2Cu^{II}_2$[a] superoxide dismutase	$[Cu(im)_4]^{2+}$ [b]	blue copper[c]
N1: A_x = 45–48, A_z = 39	41	N1: 32–39
N2: A_x = 23–29, A_z = 28–32		N2: 16–24

[a] Present results. The N1 coupling is associated with one histidyl imidazole, the N2 coupling with two. [b] Reference 13; coupling is essentially isotropic and all four ^{14}N are equivalent. [c] Ranges for the two observed couplings in six type 1 copper centers; ref 14. Couplings are approximately isotropic.

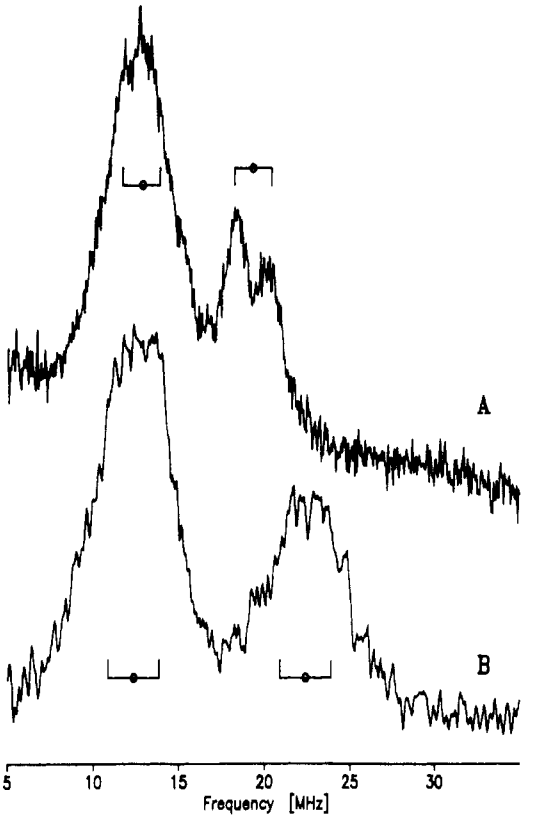

Figure 4. X-band pulse POSHE–ENDOR spectra taken at (A) the low-field edge and (B) the high-field edge of the EPR spectrum. Conditions: 9.17 GHz, $t_p(\pi)$ = 32 ns; t_{RF} = 15 μs; RF power, 200 W; 256 points/spectrum; (A) 0.2810 T; τ_{12} = 1.376 μs; 1024 transients; 14 Hz; (B) 0.3190 T; τ_{12} = 1.364 μs; 256 transients; 10 Hz.

(42) Roberts, J. E.; Brown, T. G.; Hoffman, B. M.; Peisach, J. *J. Am. Chem. Soc.* **1980**, *102*, 825–829.
(43) Rist, G. H.; Hyde, J. S.; Vanngard, T. *Proc. Natl. Acad. Sci. U.S.A.* **1970**, *67*, 79–86.

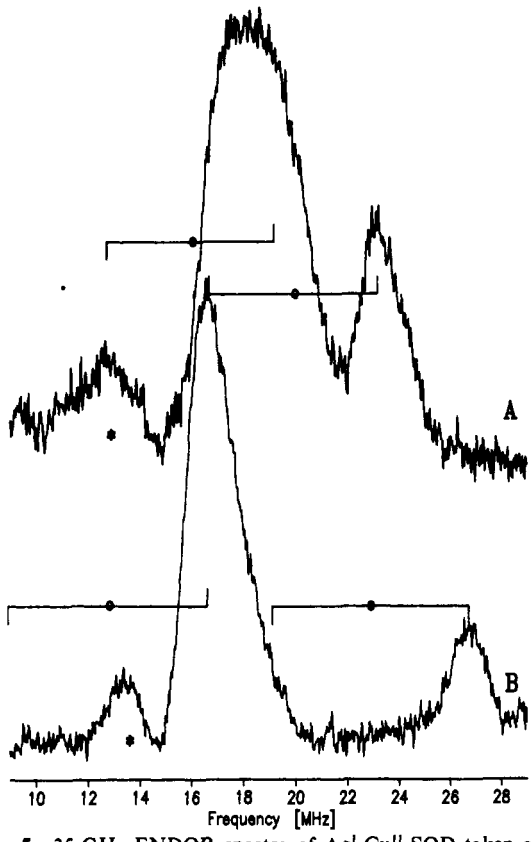

Figure 5. 35-GHz ENDOR spectra of $Ag^{I}_2Cu^{II}_2$SOD taken at field positions corresponding to those of Figure 3: (A) H = 1.07 T; (B) H = 1.25 T. Conditions are as for Figure 3 except for RF scan rate, 2 MHz/s.

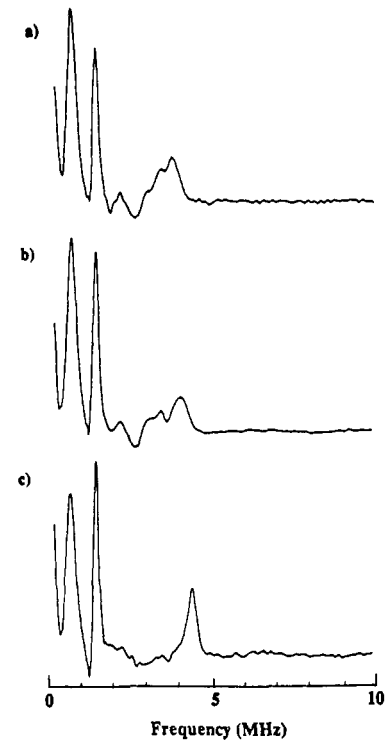

Figure 6. ESEEM spectra obtained for $Ag^{I}_2Cu^{II}_2$SOD at (a) g = 2.29; (b) g = 2.15 and (c) g = 2.02. The conditions common to all three measurements were as follows: microwave frequency, 8.681 GHz; microwave pulse power, 50 W (20 ns fwhm); sample temperature, 4.2 K; pulse sequence repetition rate, 200 Hz; and each time point represents the average of 50 events. For (a) H = 2707 G, τ = 174 ns; for (b), H = 2883 G, τ = 163 ns; and for (c) H = 3084 G, τ = 152 ns.

coordinating histidyl ligands associated with the Zn site, this requires that there are two N2 nitrogens and one N1. The breadth of the N2 feature, along with its lack of the resolved Larmor splitting as seen for N1, suggest that the two N2 nitrogens are slightly inequivalent.

Q-Band ENDOR. Figure 5 shows single-crystal-like Q-band ^{14}N ENDOR spectra taken at the low-field (g_3) and high-field (g_1) edges of the EPR envelope. The ENDOR spectrum at the low field edge (Figure 6a) consists of a strong, broad (>3 MHz) peak centered at $\nu \approx 18$ MHz and a weaker peak at $\nu \approx 23$ MHz. The assignment of the 23 MHz peak as ν_+ of a Larmor-split pair for N1 (eq 1) gives A_3(N1) ≈ 39 MHz, in agreement with the X-band results. That peak cannot be a ν_- feature, because its ν_+ partner would lie at 30 MHz and should be stronger, yet is not observed. According to eq 1 the ν_- peak for N(1) would fall at 16 MHz, at the low-frequency side of the strongest ENDOR feature.

The feature at $\nu \approx 18$ MHz is immediately assignable as being primarily associated with ν_+ for a second class of nitrogen(s), as seen in the pulsed ENDOR data; the ν_- partner of this feature is predicted to fall at $\nu \sim$ 12–14 MHz, and is barely visible. The breadth of the peak is consistent with the suggestion that it is associated with two, slightly inequivalent N2 nitrogens.

The spectrum recorded at the high-field (g_1) edge of the EPR envelope (Figure 5b) consists of a strong, slightly asymmetric peak at $\nu \approx 17$ MHz, a much weaker peak at $\nu \approx 27$ MHz and a third feature at ~13 MHz. An interpretation of the first two as ν_+ peaks from two classes N2 and N1, respectively, yields the hyperfine coupling of A_1(N1) ≈ 46 MHz and A_1(N2) ≈ 26 MHz. The coupling for N1 is in good agreement with both cw and Davies ENDOR results at X band; the signals from N2 are totally obscured by ^{1}H resonances in the cw X-band experiment, but were seen in pulsed ENDOR. One might speculate that the peak at $\nu \approx 13.3$ MHz could be a part of yet another nitrogen pattern. However, ν = 13.3 MHz corresponds to the Larmor frequency of ^{13}C and we assign this feature to distant ENDOR from ^{13}C in natural abundance, as seen in a series of Fe–S proteins.[44] As the low-field and high-field edges of the EPR envelope of $Ag^{I}_2Cu^{II}_2$SOD fall outside the envelope of native $Cu^{II}_2Zn^{II}_2$SOD, these Q-band spectra confirm that contributions from the latter are negligible.

X-Band ESEEM. ESEEM spectra collected near the principal g-values of $Ag^{I}_2Cu^{II}_2$SOD are shown in Figure 6. All three spectra show sharp lines at 0.7 and 1.4 MHz, and a broad component with a center frequency that shifts from 3.6 MHz at g = 2.29 (Figure 6a) to 4.3 MHz at g = 2.01 (Figure 6c). These spectral features are characteristic of ESEEM arising from remote, protonated, nitrogen of imidazole bound equatorially to Cu(II) and have been characterized in detail for powder samples by Mims and Peisach.[17] Briefly, the appearance of the frequency spectra shown in Figure 6 is a consequence of the Fermi contact interactions for ^{14}N being nearly equal to twice the nuclear Zeeman frequency. Under these conditions, the energy level splittings for one of the superhyperfine manifolds, where electron–nuclear hyperfine and nuclear Zeeman terms subtract from one another, are dominated by the nuclear quadrupole interaction (nqi).[51] Because the nqi is independent of magnetic field strength and direction, one expects to observe three sharp resonances from this manifold with the two lower frequency components adding to give the third. NQR measurements for imidazole and histidine powders[45] predict that for the remote nitrogen these frequencies will be 0.66, 0.76 and 1.41 MHz, in good agreement with those determined by ESEEM (Figure 6), where the predicted lower frequency features are often not resolved from one another.

(44) Houseman, A. L. P.; Oh, B.-H.; Kennedy, M. C.; Fan, Ch.; Werst, M. M.; Beinert, H.; Markley, J. L.; Hoffman, B. M. *Biochemistry* **1992**, *31*, 2073–2080.
(45) Edmonds, D. T.; Summers, C. P. *J. Magn. Reson.* **1973**, *12*, 134–142.
(46) VanCamp, H. L.; Sands, R. H.; Fee, J. A. *Biochim. Biophys. Acta* **1982**, *704*, 75–89.

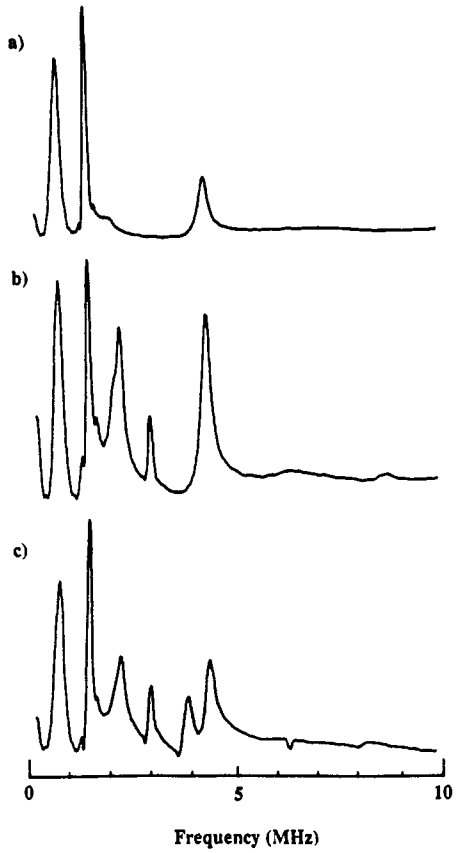

Figure 7. ESEEM spectral simulations using the procedure described in the text. Slight modifications of the reported spin Hamiltonian parameters[7] were employed: $g_1 = 2.315, g_2 = 2.125, g_3 = 2.00, A_1 = 340$ MHz, $A_2 = A_3 = 50$ MHz. Experimental parameters as described for Figure 6c were used as input values for the calculations. For (a) only a single ^{14}N nucleus is considered, while for (b) and (c), two ^{14}N nuclei give rise to the ESEEM.

For the other superhyperfine manifold, where hyperfine and nuclear Zeeman terms are additive, one typically observes broader spectral features with the only resolvable components occurring at approximately twice the ^{14}N nuclear Zeeman frequency plus an angle-selected, electron–nuclear hyperfine coupling term (roughly a $\Delta m_I = 2$ transition).

Simulation of these ESEEM data were carried out using the software described by Cornelius et al.[40] This procedure requires prior simulations of the cw-EPR spectrum of Figure 1a so that the orientations selected at the particular g-value of a measurement can be determined. ESEEM calculations focused on predicting the frequencies, relative amplitudes, and damping factors (line widths) of the three major spectral features, the sharp lines at 0.7 and 1.4 MHz, and the broad component that moves as a function of the effective g-value of the measurement. The more minor spectral features observed near 2.1 and 3.2 MHz in Figure 6a,b, were assumed to arise mostly from a population of weaker coupled ^{14}N nuclei and will be discussed below. The major spectral features of the ESEEM data collected for $Ag^{I}_2Cu^{II}_2SOD$ are best accounted for by an ^{14}N nucleus with the following coupling parameters: $A_{iso} = 2.0$ MHz; $r_{eff} = 2.85$ Å; $\theta_n = 105°$; $\phi_n = 34°$; $e^2qQ = 1.44$ MHz; $\eta = 0.94$.

A simulated ESEEM spectrum for the data collected at $g = 2.01$ (Figure 6c) is shown in Figure 7a. The value obtained for A_{iso} is similar to that found for the remote nitrogen of imidazole in Cu(II) imidazole model compounds. As the couplings for the coordinated nitrogen in those models are $A(N) \sim 41$ MHz,[15] similar to $A(N1)$ as measured here by ENDOR, we conclude that the major ESEEM frequency components arise from the population of stronger coupled imidazole ligand(s) whose directly coordinated nitrogen is observed by ENDOR.

Absent from the ESEEM spectra on Figure 6 are components arising from combination frequencies of the 0.7 and 1.4 MHz spectral lines that are expected to appear in stimulated echo or 3-pulse ESEEM spectra when two or more magnetically equivalent nuclei interact with the paramagnetic center.[21] These combination frequencies are present when Cu(II) is coordinated to more than a single imidazole, and become more prominent in the ESEEM spectrum as their number increases. Combination frequencies have been observed for model compounds Cu^{II}(imidazole)$_4$ (17) and Cu^{II}(2-methylimidazole)$_4$[21] and for several Cu(II) proteins including galactose oxidase,[47] phenylalanine hydroxylase,[21] and $Cu^{II}_2Zn^{II}_2SOD$.[17]

Figure 7b,c shows spectral simulation of the ESEEM data expected at $g = 2.01$ (Figure 6c) for the case where two ^{14}N nuclei with the same magnetic coupling strengths, but different nuclear orientations with respect to the Cu(II) **g**-tensor, are present. For Figure 7b, the direction of the hyperfine tensor principle axis with respect to the **g**-tensor is given by $\theta_n = 105°$, $\phi_n = 214°$, while for Figure 7c the second ^{14}N nucleus is at $\theta_n = 105°$, $\phi_n = 124°$. For both cases, prominent combination lines at 2.1 and 2.9 MHz are predicted. As none are seen with $Ag^{I}_2Cu^{II}_2SOD$, we conclude that the population of ^{14}N giving rise to the major features of the ESEEM spectra consists of only a single strongly bound imidazole.

The second population of directly bonded ^{14}N nuclei, N2, detected by ENDOR has hyperfine splitting parameters that are about 50% of those found for the stronger coupled ^{14}N. If this second population of ^{14}N nuclei is due to bound imidazole, then one would expect the maximum value for the contact interaction between Cu(II) and the remote nitrogen to be also reduced by about 50%, to approximately 1 MHz. ESEEM theory predicts that under these conditions the envelope modulation depths due to a single ^{14}N nucleus would be shallow giving rise to minor components in the ESEEM frequency spectrum at roughly 0.9, 2.1 and 3.3 MHz provided that the other Hamiltonian parameters used to generate the results given in Figure 7 remain unchanged. Given the presence of a single strongly bound imidazole, the only resolvable components would be observed from 2 to 3.5 MHz. Examination of Figure 6 shows minor components in this range. However, the signal-to-noise ratio for the data is such that no conclusive statement concerning the number of nuclei that give rise to these spectral features can be made.

Discussion

A combination of X- and Q-band cw and pulsed ENDOR techniques has clearly shown that Cu(II) substituted in the Zn site of SOD shows two distinct types of coordinated nitrogen. Nitrogenous ligand N1 has a hyperfine coupling with tensor values in the range $39 \leq A(N1) \leq 46$ MHz. The isotropic coupling constant, $A(N1) \approx 42$ MHz, is similar to that seen for imid equatorially bound to Cu(II) in a site with near-D_{4h} symmetry. A second class of nitrogen ligand, comprised of two members, with hyperfine couplings roughly $^1/_2$–$^2/_3$ that for N1 also was found.

ENDOR studies of blue copper proteins,[16] show both a large ($A \sim 32$–49 MHz) and a small ($A \sim 16$–24 MHz) ^{14}N coupling to copper (Table I). In line with ESEEM results,[18] the larger coupling derived from ENDOR was assigned to a more or less normal imidazole, strongly bound to Cu(II). It was suggested[16] that the coupling to the second imidazole is reduced because of unfavorable electronic overlap of ^{14}N with the metal ion. As a limiting case of such geometric discrimination, in tetragonal Cu(II) complexes axial ^{14}N is coupled about 20 times less than equatorial ^{14}N.[40]

As a reference for the present ESEEM data for $Ag^{I}_2Cu^{II}_2$-SOD, we recall the ESEEM results for the native enzyme, Cu^{II}_2-

(47) Kosman, D. J.; Peisach, J.; Mims, W. B. *Biochemistry* **1980**, *19*, 1304–1308.

Zn^{II}_2SOD.[19] The frequency spectrum of the latter consists of intense, sharp lines at 0.5, 0.9, 1.05, 1.35, and 1.55 MHz, a broad peak centered at 3.9 MHz, and weak combination lines at 0.2, 1.8–2.1, 2.4, and 2.9 MHz. These data were interpreted as arising from the remote nitrogens of two magnetically distinct populations of imidazole ligands bound to Cu(II). Specific removal of Zn(II) from native enzyme results in ESEEM spectra that consist of broad lines centered at 0.75 and 4.0 MHz, a sharp line at 1.55 MHz, and weak combination lines at 2.3 and 3.1 MHz. The presence of these combination lines and the amplitude of the 4.0-MHz peak indicate that all three imidazole groups are still bound but that their magnetic couplings to Cu(II) are now more equivalent as a result of the disruption of the imidazolate bridge.

The ESEEM spectrum for $Ag^{I}_2Cu^{II}_2$SOD, contains 3 sharp lines rather than the multiplicity of lines seen for $Cu^{II}_2Zn^{II}_2$SOD. As no combination frequencies are seen, this suggests that only a single imidazole gives rise to the spectrum.[21] These differences provide further proof that Cu(II) occupies the Zn(II) site in $Ag^{I}_2Cu^{II}_2$SOD and that contributions from residual $Cu^{II}_2Zn^{II}_2$SOD to our ENDOR and ESEEM data are negligible. Comparison with ENDOR and ESEEM studies of $Cu^{II}(imid)_4$[8,17] indicate that this imidazole is the one whose directly coordinated ^{14}N is N1, the one with the greater ENDOR frequency. It is unlikely that this imidazole forms a bimetallic bridge, as the ESEEM frequencies for the remote ^{14}N are those of protonated imidazole. These frequencies would likely shift, as they do in $Cu^{II}_2Zn^{II}_2$SOD, if the remote nitrogen was coupled to a metal ion in the same fashion as Zn(II) in the native protein.[19] Combining this with the ENDOR data we may conclude then, that all three imidazoles are bound to Cu(II), and that the bimetallic bridge between Cu(II) and Ag(I) is not formed. This is in agreement with the suggested mechanism of catalysis for the native protein, which postulates that the bimetallic bridge is broken when a univalent metal occupies the copper binding site.[48]

The presence of inequivalent imidazole ligands to Cu(II) likely is due to the pseudo-tetrahedral geometry of the three histidine imidazoles and the single carboxylate sidechain (from Asp 81) that make up the zinc binding site. The bonding orbitals for Cu(II) favor near tetragonal symmetry and our results suggest that only a single imidazole ^{14}N aligns with and is strongly bonded to the half-filled Cu(II) $d_{x^2-y^2}$ orbital, and that the other two imidazole ^{14}N are bent away as is seen in blue copper proteins, resulting in diminished orbital overlap. Thus the presence of both normal and weak imidazole interactions is a consequence of constraint on coordination geometry imposed by the protein superstructure.

This does not mean that multi-imidazole coordination to Cu(II) in a near tetrahedral site must necessarily lead to inequivalent ^{14}N coupling, nor does it require that imidazole–^{14}N coupling to Cu(II) in a tetragonal site need be equivalent. For example, in a single-crystal ESEEM study of Cu(II)-doped Zn(II) (1,2-dimethylimid)$_2Cl_2$,[49] where Cu(II) occupies a near tetrahedral site, the electron–nuclear coupling from the remote ^{14}N of both coordinated dimethylimidazoles to Cu(II) is essentially the same. On the other hand, where Cu(II) is bound to isopenicilline synthase, bis(imidazole) coordination to the nearly tetragonal Cu(II) is indicated, but with inequivalent coupling to the remote ^{14}N.[50]

In the case of the blue copper proteins such as stellacyanin, where two imidazole nitrogens show inequivalent coordination to metal,[14] the ESEEM spectrum also is dominated by lines arising from the remote ^{14}N of the single, tightly coupled imidazole, with spectral properties resembling those seen for Cu^{II}(diethylenetriamine)(imid).[17] However, careful examination of the published ESEEM spectrum for stellacyanin shows that a weaker line at 3.2 MHz is also present (ref 18, Figure 2B) and this is now attributed to the remote ^{14}N of the more weakly coupled imidazole. ESEEM spectral simulations carried out assuming contact interactions half that seen for normal Cu(II)–imid complexes essentially duplicates the published spectrum for stellacyanin. In $Ag^{I}_2Cu^{II}_2$SOD, couplings of this type may be present in the ESEEM spectrum, although not as well resolved as in stellacyanin.

Finally, the unusual Cu(II) EPR spectra of $Ag^{I}_2Cu^{II}_2$SOD and of the magnetically uncoupled type 3 copper of tree laccase[12] are similar and it appears that both bind three imidazoles, but the present data show that the imidazole binding differs markedly. The ENDOR results for the latter show no small nitrogen hyperfine coupling of the N2 type, as observed in the former and in blue copper sites. It may well be that any geometric constraints that would lead to a strong inequivalence among the bonds to the native type 3 Cu(II) are relaxed in the uncoupled binuclear system.

Acknowledgment. This work has been supported by the NIH (GM28222, J.S.V.; HL13531, B.M.H.; GM40168, RR02583, J.P.; GM45795, J.Mc.C.) and by the NSF (DBM-8907559, B.M.H.). The technical expertise of Mr. Clark E. Davoust and helpful discussions with Professor James A. Roe are greatly appreciated.

(48) Steiman, H. M. In *Superoxide Dismutase*; Oberley, L. W., Ed.; CRC Press: Boca Raton, FL, 1982; Vol. 1, pp 11–68.

(49) Colaneri, M. J.; Potenza, J. A.; Schugar, H. J.; Peisach, J. *J. Am. Chem. Soc.* **1990**, *112*, 9451–9458.

(50) Jiang, F.; Peisach, J.; Ming, L.-J.; Que, L.; Chen, V. J. *Biochemistry* **1991**, *30*, 11437–11445.

(51) Jiang, F.; McCracken, J.; Peisach, J. *J. Am. Chem. Soc.* **1990**, *112*, 9035–9044.